STM JOURNALS

Research & Reviews: Journal of
Computational Biology

https://journals.stmjournals.com/rrjocb/

ISSN: 2319-3433 (Online)
ISSN: 2349-3720 (Print)
Volume 15, Issue 1, 2026
January–April
DOI (Journal): 10.37591/RRJoCB

Research RRJOCB

Computational Exploration of *Aristolochia indica* Bioactive Compounds Against Snake Venom Proteins Using Docking and Dynamics Simulations

Sidharth Pottangadi*

Abstract

Snakebite envenoming is a neglected health threat impacting millions of people each year, especially in tropical and subtropical countries. Ethnomedicinal plants are sources of various bioactive compounds and have been utilized by several tribes across the world for centuries. Aristolochia indica is a perennial herb mentioned in Indian Ayurveda with a long history of use against snake venom, scorpion venom, fevers, rheumatic arthritis, liver ailments, leishmaniasis, etc. The major bioactive compounds used as a traditional source of antivenom from this plant are aristolochic acids and aristolactams and have been recently found to be nephrotoxic and mutagenic. Here, attention is brought to other phytocompounds from A. indica with the potential to act as antivenom proteins. Through docking using Autodock 4.0, it was found that phytocompounds from A. indica, namely, cubebin, hinokinin, ishwarol, and ledol, possess high binding affinity towards major venom proteins. These phytocompounds were found to interact with the amino acid residues at the active site of venom proteins, which could compromise their binding and function. Molecular dynamics simulations further determined the structural stability of the L-amino acid oxidase–cubebin complex. This study, therefore, provides insight into new compounds that have the potential to replace conventional snake antiserum therapy.

Keywords: *Aristolochia indica*, phospholipase A2, metalloproteinases, L-amino acid oxidase, three-finger toxins

INTRODUCTION

Snakes are remarkable creatures that have been inhabiting the planet long before ancient humans walked on the Earth [1]. They are limbless creatures capable of immobilizing/killing prey using the venom they produce or by constricting them and are adept at swallowing prey much larger than themselves [2]. It is believed that venom evolved over the centuries in accordance with their prey physiology. Hence, the central constituents of venom may differ between each species of a genus and are also dependent on other factors, including habitat, size, and age of the snake [3].

***Author for Correspondence**
Sidharth Pottangadi
E-mail: sidharthpottangadi@gmail.com

Student, Department of Bioinformatics, BioNome, Bengaluru, Karnataka, India

Received Date: November 02, 2025
Accepted Date: February 07, 2026
Published Date: February 14, 2026

Citation: Sidharth Pottangadi. Computational Exploration of *Aristolochia indica* Bioactive Compounds Against Snake Venom Proteins Using Docking and Dynamics Simulations. Research & Reviews: Journal of Computational Biology. 2026; 15(1): 50–66p.

Snake venom (SV) is a complex cocktail of bioactive proteins and polypeptides and is known to target various physiological systems and cause neurotoxic or hemotoxic effects on its prey. Most of these proteins exist as monomers but are capable of forming covalent and non-covalent complexes, enhancing the lethal potency of the toxin [4]. These proteins and polypeptides can be classified as enzymatic (phospholipase A2, L-amino acid oxidases, metalloproteinases, and serine proteases) and non-enzymatic (three-finger toxins, disintegrins, and Kunitz peptides) [5]. Phospholipase A2s (PLA2s) are a major constituent

© STM Journals 2026. All Rights Reserved

of most snake venoms and act by targeting the sn-2 position in a Ca2+-dependent manner, hydrolyzing phospholipids in cell membranes and releasing fatty acids and lysophospholipids [5]. These protein complexes also bind to the presynaptic site at neuromuscular junctions and decrease the release of acetylcholine to interrupt neurotransmission [4]. Snake venom metalloproteinases (SVMPs) and serine proteases (SVSPs), on the other hand, function almost similarly by activating prothrombin/coagulation factor X of the blood coagulation pathway, thereby degrading fibrinogen and ultimately inhibiting platelet aggregation, causing haemorrhages, blistering, and tissue necrosis [6]. L-amino acid oxidases (LAAOs) are flavoenzymes that catalyze the conversion of L-amino acids to α-keto acids through oxidative deamination, releasing ammonia and hydrogen peroxide. The hydrogen peroxide released in this process is believed to cause toxic effects [4]. Three-finger toxins (3FTx) are non-enzymatic proteins that disrupt nerve and muscle function by targeting postsynaptic nicotinic and muscarinic acetylcholine receptors, leading to a loss in nerve–muscle communication, ultimately causing skeletal muscle paralysis and respiratory failure [7]. The composition of these venom proteins may vary amongst genera/species; for example, in elapids, the major constituents are 3FTx and PLA2. On the contrary, the venom of vipers consists of PLA2, SVSP, and SVMP but almost lacks 3FTx [5]. This variation in the composition and function of snake venom makes it a challenging drug target and makes it difficult to achieve promising efficacy.

The consequences of snakebites on humans can be severe, although humans are not considered prey for snakes. Nevertheless, humans are often attacked by snakes as an act of defence, especially among rural, impoverished populations in the tropics [3]. Snake envenomation is, therefore, turning into a major concern worldwide, especially in tropical and subtropical countries. Each year, there are more than 440,000 cases of envenomation and 20,000 deaths [8, 9]. Antivenom, obtained from purifying antibodies (immunoglobulin G) from hyper-immunized animals on administration of different snake venoms, offers an effective mode of treatment. Even though antivenoms provide sufficient treatment effects, the specificity of the antibodies often results in reduced recognition of venom from different species. The mortality rate remains high due to the limited therapeutic efficacy, unavailability, and safety concerns of using antivenoms [9]. Therefore, there is an increasing need to develop new therapeutic drugs/compounds that can counteract the toxic effects of venom proteins or work synergistically with conventional antivenom.

Humans have depended on plants as an essential source of medicine since time immemorial. Many countries, like India, China, Japan, Africa, etc., have been practicing the use of herbal medicines for thousands of years. In fact, the World Health Organization has recognized traditional sources of medicine as a valid therapy for various human diseases [9]. In India, Ayurveda, Unani, Siddha, Tibbi, and Homoeopathy have been popularly practised [9]. The plant *Aristolochia indica* has been part of the traditional Ayurvedic system of medicine for a very long time. It has been used extensively in treating snakebites and has also been used against cholera, pneumonia, fevers, rheumatic arthritis, gastric problems, leprosy, skin diseases, leishmaniasis, and sexual diseases [10]. A wide range of phytocompounds, including aristolochic acids, aristolactams, phenanthrenes, terpenes, alkaloids, lignans, and steroids, are found in this species [11]. The major phytocompound, aristolochic acid (AA), from the plant was found to exert anti-snake-venom properties by acting as a potential inhibitor of PLA2, acetylcholinesterase, and plasma proteases [10]. However, during the metabolism of AA, cytoplasmic enzymes activate it to form aristolactams, which form covalent adducts with DNA to form dA-aristolactams and dG-aristolactams. The former adduct is a potent carcinogen and nephrotoxin [12]. Therefore, the use of AA as a therapeutic strategy is not advised and is considered dangerous; yet this practise continues in many Southeast Asian countries against snake venom.

The particular interest of this in silico study is to identify phytocompounds that can be isolated from *A. indica* and offered as a suitable substitute for AA. Here, 58 phytocompounds that are present in the plant were retrieved from an online database. The physicochemical and pharmacological properties were analyzed, and the top ligands that met the criteria for the study were subjected to molecular

© STM Journals 2026. All Rights Reserved

docking. Furthermore, a molecular dynamics simulation was performed to assess the stability of the SV protein–ligand complex. This study, therefore, provides insight into phytocompounds with the potential to replace conventional snake antiserum therapy with a much more effective alternative treatment.

METHODS

Retrieval of Phytocompounds

The IMPPAT (Indian Medicinal Plants, Phytochemistry, and Therapeutics) database (https://cb.imsc.res.in/imppat/) was used to retrieve phytocompounds from the medicinal plant *Aristolochia indica* (Indian birthwort) that may possess potential antivenom properties. Fifty-eight such phytocompounds from *Aristolochia indica* were considered for this study. The canonical SMILES, PubChem CID, and two-dimensional (2D) models of these phytocompounds in SDF format were retrieved from the PubChem database (https://pubchem.ncbi.nlm.nih.gov/).

Retrieval of Venom Proteins

Three-dimensional structures of the targeted venom proteins were obtained from the Research Collaboratory for Structural Bioinformatics Protein Data Bank (PDB) (https://www.rcsb.org/) in legacy PDB format. The following proteins were considered as common components of snake venom, and all proteins were resolved using X-ray diffraction: phospholipase A2 (PLA2) (1A3F, 2.65 Å), snake venom metalloproteinases (1ND1, 1.93 Å), three-finger toxins (5XWE, 1.80 Å), and snake venom L-amino acid oxidase (4E0V, 3.10 Å).

Protein Structure Validation

The Ramachandran plot was used to analyze the torsional angles (psi and phi) of the purified protein structure to assess its quality. The plots were obtained from PDBsum Generate (https://www.ebi.ac.uk/thornton-srv/databases/pdbsum/Generate.html). The Ramachandran plot was created using PROCHECK, and the quality was assessed based on the percentage of amino acids in favorable, additionally allowed, generously allowed, and disallowed zones.

In Silico Pharmacological Studies

To assess the pharmacological characteristics of the phytocompounds, SwissADME (http://www.swissadme.ch/) was used. The ADME analysis predicts physicochemical properties, medicinal chemistry, and pharmacokinetic parameters (absorption, distribution, metabolism, excretion, and toxicity) to determine the compound's potential as a possible drug candidate. The toxicity of the phytocompounds was assessed using the ProTox-II tool (https://tox.charite.de/protox3/index.php?site=compound_input) by adding their respective canonical SMILES and selecting all possible targets.

Protein Purification

All the selected venom proteins were purified before docking using DS BIOVIA Discovery Studio [13]. Water molecules, non-essential ligands, and heteroatoms were removed in this process to improve the efficiency and accuracy of the docking process. To further simplify the protein structure, additional chains were removed, and only the A chain was retained. Polar hydrogen atoms were added in the end to improve hydrogen bonding in the purified structure. The purified structures of the proteins were saved as PDB files.

Molecular Docking and Visualization

The PyRx virtual screening tool software [14] was used to evaluate the phytocompounds as potential venom protein inhibitors. Five phytocompounds were selected as ligands to dock against each venom protein independently. The purified venom proteins were added as macromolecules; subsequently, ligands were added, and energy minimization was performed by applying the universal force field using the OpenBabel feature. The loaded ligands were then converted from SDF into PDBQT format. The grid dimensions were generated for each protein: phospholipase A2 (X: 43.6007 Å, Y: 28.5826 Å, Z: 36.8574 Å), metalloproteinase (X: 46.2297 Å, Y: 46.1435 Å, Z: 47.0919 Å), L-amino acid oxidase (X: 71.2282 Å, Y: 52.8449 Å, Z: 66.6674 Å), and three-finger toxin (X: 31.5261 Å, Y: 26.2719, Z: 24.9659

© STM Journals 2026. All Rights Reserved

Å). The ligands were then docked with each protein, and the binding affinity corresponding to zero root-mean-square deviation (RMSD) values were recorded. The top three ligands with the lowest binding affinities were considered the best conformation of the ligand and were, thereby saved in PDB format and visualised in DS BIOVIA Discovery Studio. The protein–ligand interactions in 2D and 3D were investigated.

Molecular Dynamics Simulations

Molecular dynamics simulations (MDS) serve as an essential tool in computational biology for assessing the temporal stability and interaction dynamics of biomolecular complexes. For this investigation, the GROMACS simulation software was utilized to study the dynamics of the complex.

The simulation was initiated with the generation of a precise topological model for the GROMOS96 54a7 force field. The widely adopted GROMOS96 54a7 force field for the protein and the SwissParam force field for the ligand simulate the molecular forces and dynamics, encapsulating the complex in a cubic simulation box with dimensions on each side to simulate a naturalistic molecular environment. Initial system preparation involved an energy minimization step using the steepest descent method to minimize potential energy.

This was followed by the introduction of the Single Point Charge Extended (SPCE) water model for system solvation, and appropriate concentrations of sodium and chloride ions were added to replicate physiological ionic conditions and a balanced pH.

The equilibration phase was divided into two segments. Initially, a 10-nanosecond temperature equilibration was conducted under the NVT ensemble using the V-rescale temperature coupling method, stabilizing the system at 300 K. This phase included positional restraints to ensure proper orientation of solvent molecules around the complex.

It was succeeded by a 10-nanosecond pressure equilibration phase under the NPT ensemble, where positional restraints were progressively lifted to achieve pressure stabilization. The final phase entailed a comprehensive 100-nanosecond production simulation, which is crucial for observing the naturalistic molecular motions and interactions under stable conditions of temperature (300 K) and pressure (1 bar). Throughout this period, important dynamic parameters, such as root-mean-square deviation (RMSD), root-mean-square fluctuation (RMSF), radius of gyration (ROG), solvent-accessible surface area (SASA), and hydrogen bonding (H-bond) activity, were meticulously recorded to elucidate the stability and interaction dynamics of the protein and ligand.

RESULTS

Protein Structure Validity

The Ramachandran plot was used to assess the quality of the purified venom proteins. The plot determines the energetically permissible combinations of dihedral angles (phi and psi) between amino acids in a protein structure. The percentage of amino acids falling in different regions of the Ramachandran plot and the number of glycine and proline residues for each venom protein are listed in Table 1.

Table 1. Ramachandran plot statistics of purified venom proteins.

Purified protein	Favored region (%)	Additional allowed region (%)	Generously allowed region (%)	Disallowed region (%)	Glycine residues	Proline residues
Phospholipase A2	87.5	11.5	1	0	9	2
Metalloproteinase	89	10.4	0.5	0	12	6
L-Amino acid oxidase	68.4	28.9	1.4	1.2	35	21
Three finger Toxin	87.2	12.8	0	0	6	3

© STM Journals 2026. All Rights Reserved

Phospholipase A2

The secondary structure of the purified protein and the Ramachandran plot are displayed in Figure 1(A) and (B), respectively. The PDBsum results of the secondary structure are one sheet, one beta hairpin, two strands, six helices, six helix–helix interactions, Twelve beta turns, two gamma turns, and seven disulphides. The structure contains 119 residues in total.

Metalloproteinase

The secondary structure of the purified protein and the Ramachandran plot are displayed in Figure 2(A) and (B), respectively. The PDBsum results of the secondary structure are three sheets, one beta hairpin, one psi loop, one beta bulge, nine strands, nine helices, four helix–helix interactions, Thirteen beta turns, three gamma turns, and three disulphides. The structure contains 201 residues in total.

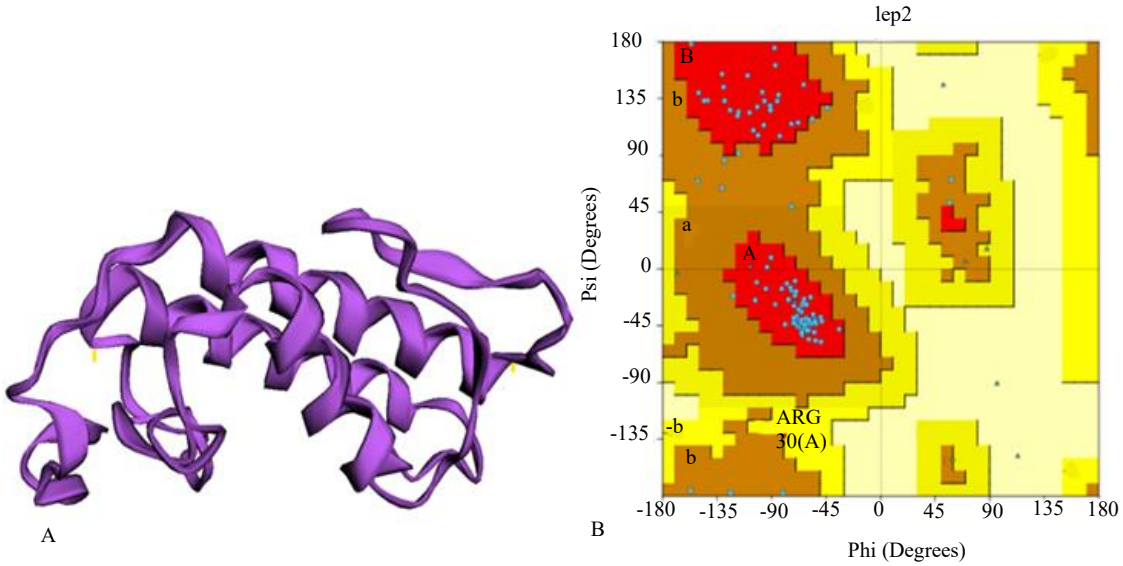

Figure 1. Structural analysis of the purified pla2 protein. (a) secondary structure of the pla2 protein. (b) Ramachandran plot of the pla2 protein.

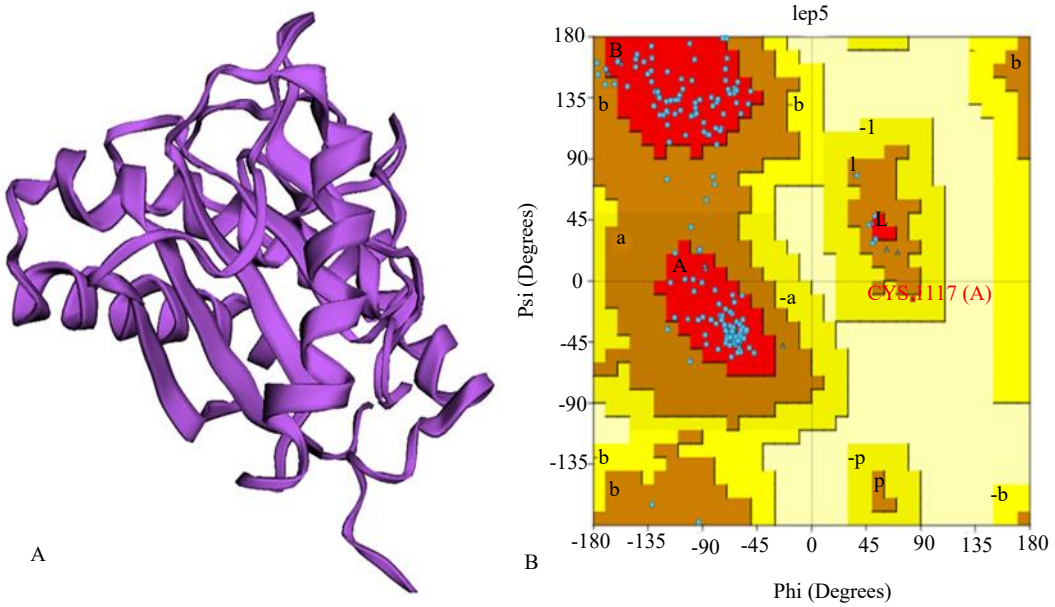

Figure 2. Structural analysis of the purified metalloproteinase protein. (a) secondary structure of metalloproteinase. (b) Ramachandran plot of metalloproteinase.

© STM Journals 2026. All Rights Reserved

L-Amino Acid Oxidase

The secondary structure of the purified protein and the Ramachandran plot are displayed in Figure 3(A) and (B), respectively. The PDBsum results of the secondary structure are five sheets, one beta–alpha–beta unit, six beta hairpins, two beta bulges, twenty-two strands, twenty-two helices, twenty-three helix–helix interactions, fifty-two beta turns, two gamma turns, and two disulphides. The structure contains 474 residues in total.

Three-Finger Toxins

The secondary structure of the purified protein and the Ramachandran plot are displayed in Figure 4(A) and (B), respectively. The PDBsum results of the secondary structure are two sheets, two beta hairpins, one beta bulge, five strands, four beta turns, and four disulphides. The structure contains 51 residues in total.

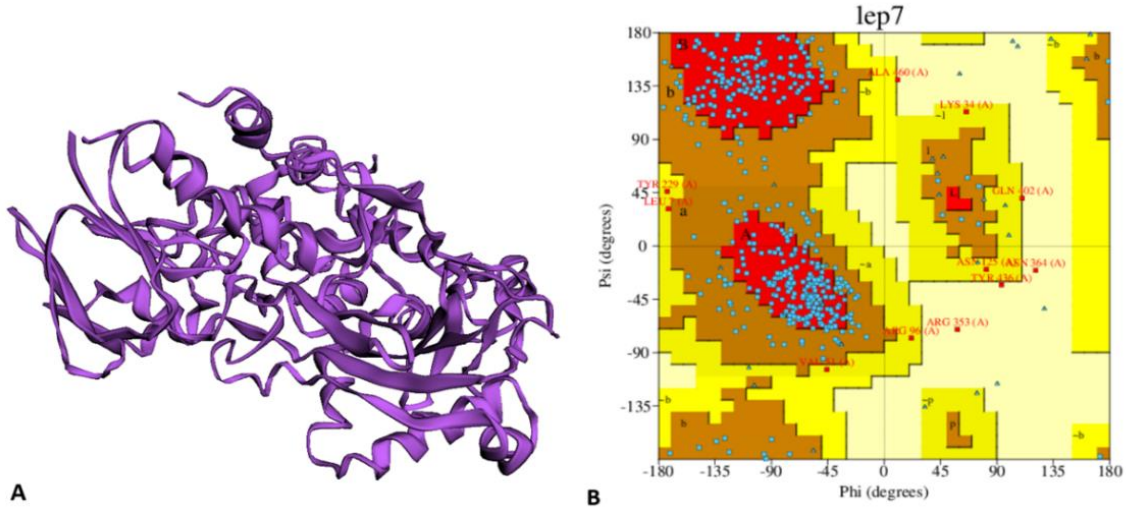

Figure 3. Structural analysis of the purified l-amino acid oxidase protein. (a) secondary structure of l-amino acid oxidase. (b) Ramachandran plot of l-amino acid oxidase.

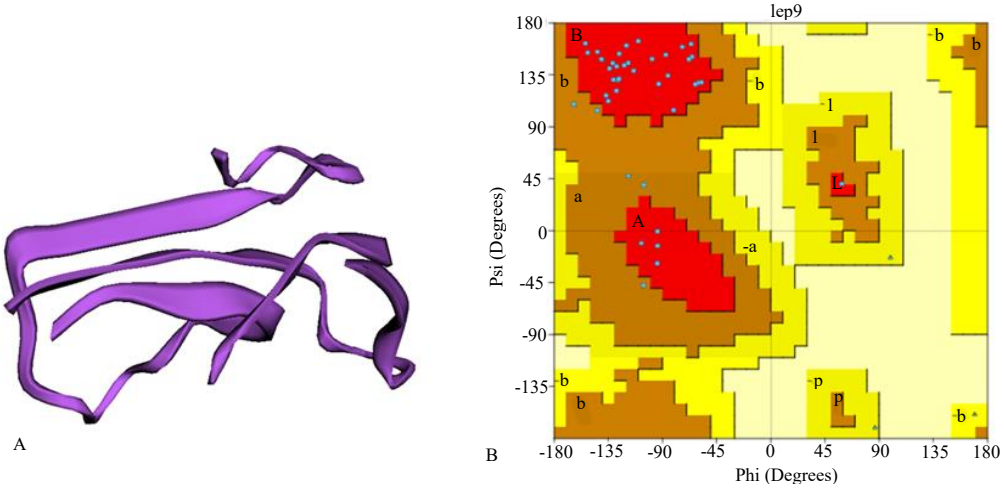

Figure 4. Structural analysis of the purified three-finger toxin protein. (a) secondary structure of the three-finger toxin. (b) Ramachandran plot of the three-finger toxin.

ADME Analysis of Phytocompounds

Physicochemical properties, ADME properties, Lipinski's rule of five, PAINS, and BRENK were considered for the evaluation of compounds capable of producing drug-like properties. Fifty-eight

© STM Journals 2026. All Rights Reserved

phytocompounds from *A. indica* were screened to determine the compounds that meet the conditions mentioned.

Physicochemical Parameters

The phytocompounds were screened based on the parameters listed in Table 2 [15], and the top five compounds that best suit these criteria are listed in Table 3.

Table 2. Physicochemical parameters [15].

Physiochemical property	Optimal range
Lipophilicity (xLogP)	−0.7 to +5.0
Size (MW)	150–500 g/moL
Polarity (TPSA)	20–130
Saturation (Sp3 hybridization)	≥0.25
Flexibility (Rotatable bonds)	≤9

Table 3. Screened phytocompounds are based on physicochemical properties.

Ligand	MW (g/moL)	Fraction csp3	Rotatable bonds	TPSA	Lipophilicity
Cubebin	356.37	0.4	4	66.38	3.38
Ishwarol	220.35	1	0	20.23	3.4
Hinokinin	354.35	0.35	4	63.22	3.65
Camphor	152.23	0.9	0	17.07	2.19
Ledol	222.37	1	0	20.23	3.74

Lipinski Filter Analysis

The five parameters listed in Lipinski's rule of five are listed in Table 4. The compounds must fulfil at least four of the parameters listed in Table 4 [15], and the top five phytocompounds that meet the specified criteria are listed in Table 5.

Table 4. Parameters for Lipinski's rule of five [15].

Properties	Optimal range
MW	150–500 Daltons
MlogP	<4.15
H donors	<5
H acceptors	<10
Molar refractivity	40–130

Table 5. Screened phytocompounds are based on Lipinski's rule of five.

Ligand	MW (g/moL)	MLogP	H donors	H acceptors	Molar refractivity
Cubebin	356.37	2.38	1	6	92.16
Ishwarol	220.35	3.81	1	1	66.14
Hinokinin	354.35	2.71	0	6	91.23
Camphor	152.23	2.3	0	1	45.64
Ledol	222.37	3.81	1	1	68.82

ADME Analysis

ADME analysis considers four characteristics: absorption, distribution, metabolism, and excretion. As shown in Table 6, all the ligands meet the criteria and possess high BBB permeability and GI

© STM Journals 2026. All Rights Reserved

absorption, exhibit good solubility, and belong to class 4 toxicity, which is considered moderate-to-low toxicity.

From the performed ADME analysis, the top five ligands, along with their PubChem CID and canonical SMILES, were listed in Table 7.

Table 6. Screened ligands based on ADME data.

Ligand	BBB	GI absorption	PGP substrate	Solubility (silicos-IT logS)	Toxicity class
Cubebin	Yes	High	No	–4.77	4
Ishwarol	Yes	High	No	–2.84	4
Hinokinin	Yes	High	No	–5.46	4
Camphor	Yes	High	No	–2.6	4
Ledol	Yes	High	No	–2.73	4

Table 7. Five screened phytocompounds/ligands for further analysis.

Ligand	PubChem CID	SMILES
Cubebin	117443	O[C@H]1OC[C@@H] ([C@H]1Cc1ccc2c(c1) OCO2) Cc1ccc2c(c1) OCO2
Ishwarol	42608203	C[C@@H]1CCC(C23[C@@]1(C)CC1C(C2) C1(C3) C) O
Hinokinin	442879	O=C1OC[C@@H] ([C@H]1Cc1ccc2c(c1) OCO2) Cc1ccc2c(c1) OCO2
Camphor	159055	O=C1C[C@@H]2C([C@@]1(C)CC2) (C)C
Ledol	92812	C[C@@H]1CC[C@H]2[C@@H]1[C@H]1[C@H] (C1(C)C) CC[C@@]2(C)O

Molecular Docking and Visualization

The five ligands were docked against each of the four venom proteins using the PyRx software, and the top three ligand conformations with the highest binding affinities (least negative values) with each protein were recorded (Table 8). The selected ligands were then visualized using Dassault Systèmes BIOVIA Discovery Studio, and the 2D and 3D structures were obtained. Furthermore, the amino acid residues involved in interacting with the ligands are labelled.

Table 8. Binding affinity of proteins with respective ligands.

Protein	Ligand	PubChem CID	Binding affinity (kcal/mol)
Phospholipase A2	Cubebin	117443	–8.5
	Hinokinin	442879	–8.2
	Ledol	92812	–5.8
Metalloproteinase	Cubebin	117443	–8.7
	Hinokinin	442879	–8.6
	Ishwarol	42608203	–6.4
L-Amino Oxidase	Cubebin	117443	–9.6
	Hinokinin	442879	–9.1
	Ledol	92812	–8.4
Three Finger Toxin	Hinokinin	442879	–6.9
	Cubebin	117443	–6.5
	Ishwarol	42608203	–5.2

Phospholipase A2

The 3D and 2D structures of PLA2 bound to cubebin are shown in Figure 5(A) and (B), respectively. The major amino acids involved in the protein–ligand complex are Gly29, Asp48, Glu55, Pro62, Tyr63, and Phe64.

© STM Journals 2026. All Rights Reserved

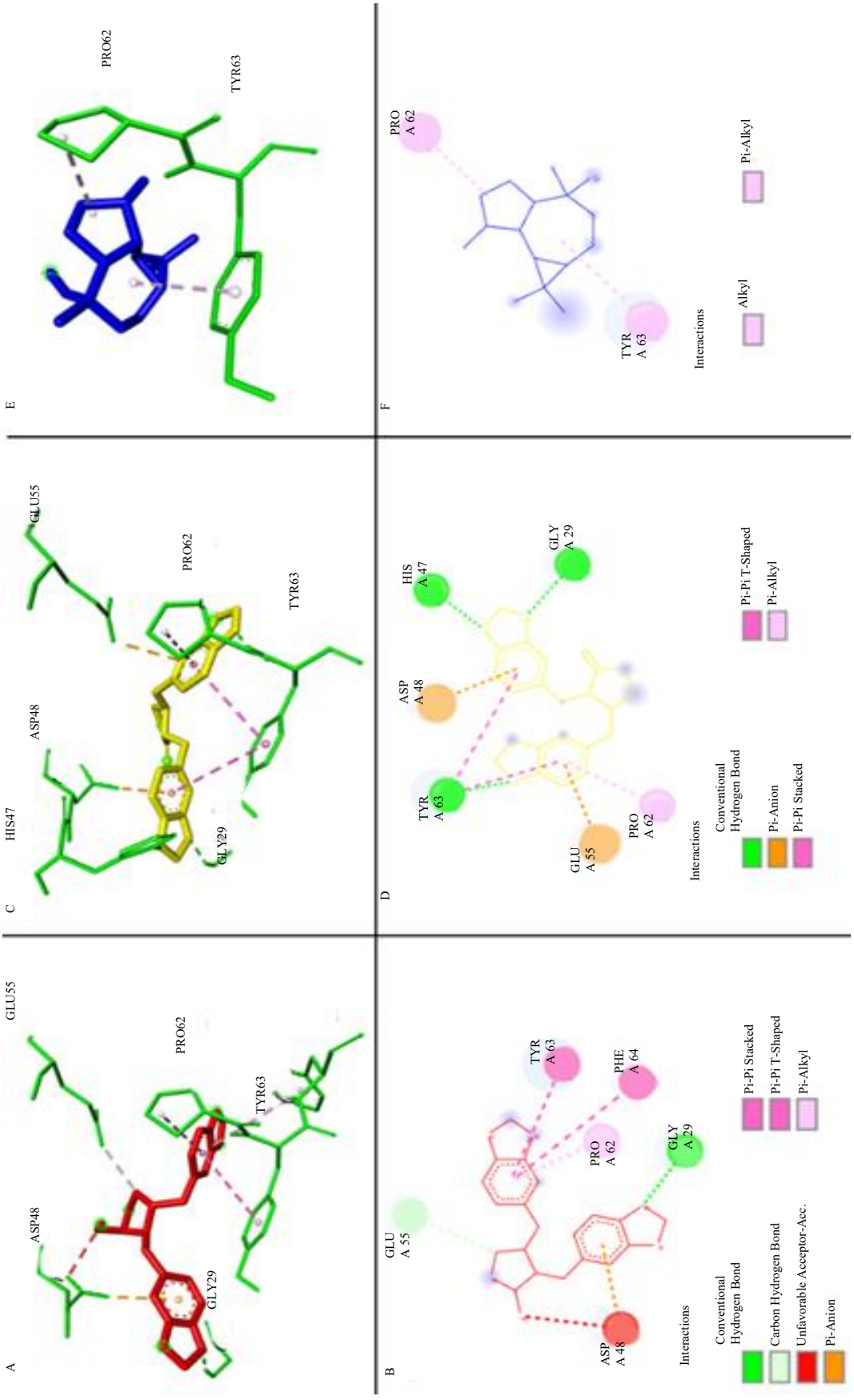

Figure 5. (a) 3d structure of the PLA2 protein (green) bound to cubebin (red). (b) 2d structure of the PLA2 protein bound to cubebin. (c) 3d structure of the PLA2 protein (green) bound to hinokinin (yellow). (d) 2d structure of the PLA2 protein bound to hinokinin. (e) 3d structure of the PLA2 protein (green) bound to ledol (blue). (f) 2d structure of the PLA2 protein bound to ledol.

© STM Journals 2026. All Rights Reserved

The 3D and 2D structures of PLA2 bound to hinokinin are shown in Figure 5(C) and (D), respectively. The major amino acids involved in the protein–ligand complex are Gly29, His47, Asp48, Glu55, Pro62, and Tyr63.

The 3D and 2D structures of PLA2 bound to ledol are shown in Figure 5(E) and (F), respectively. The major amino acids involved in the protein–ligand complex are Pro62 and Tyr63.

Metalloproteinase

The 3D and 2D structures of SVMP bound to cubebin are shown in Figure 6(A) and (B), respectively. The major amino acids involved in the protein–ligand complex are Ile108, Thr139, His142, His146, His152, Val169, and Leu170.

The 3D and 2D structures of SVMP bound to hinokinin are shown in Figure 6(C) and (D), respectively. The major amino acids involved in the protein–ligand complex are Ile108, His142, Ile165, and Leu170.

The 3D and 2D structures of SVMP bound to ishwarol are shown in Figure 6(E) and (F), respectively. The major amino acids involved in the protein–ligand complex are His142, His146, His152, and Leu170.

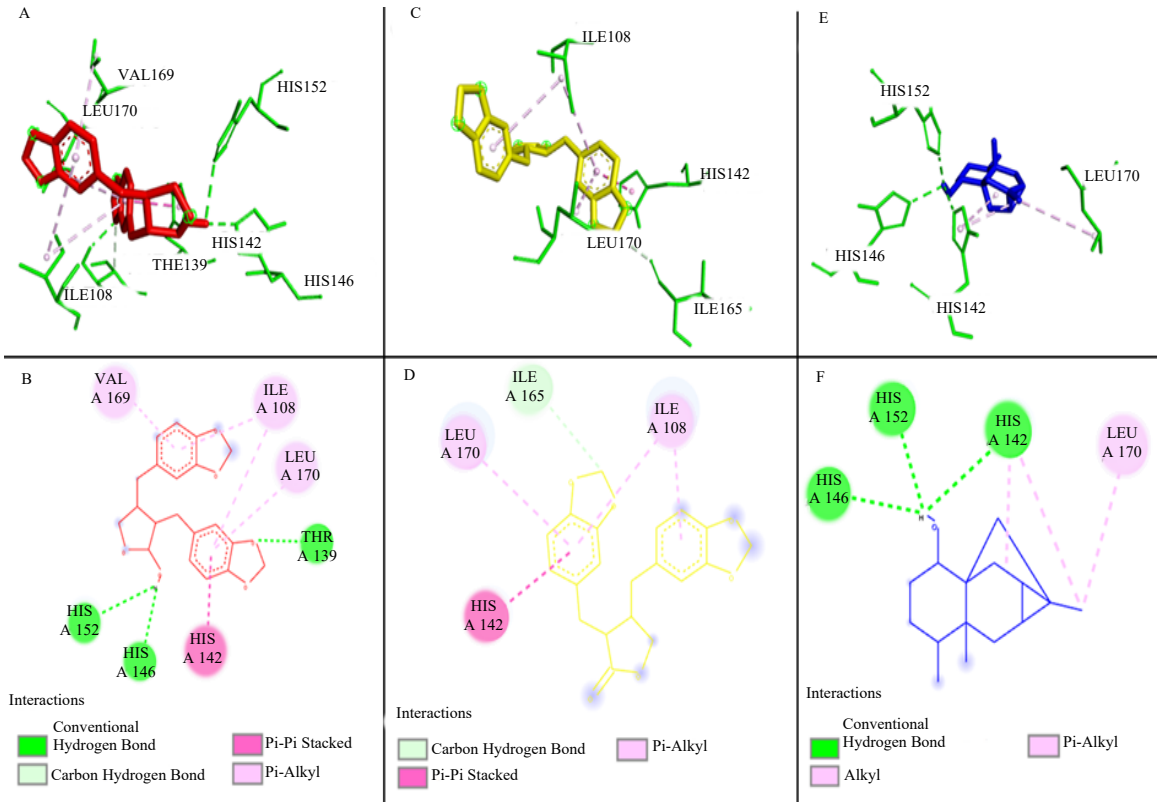

Figure 6. (a) 3d structure of the SVMP protein (green) bound to cubebin (red). (b) 2d structure of the SVMP protein bound to cubebin. (c) 3d structure of the SVMP protein (green) bound to hinokinin (yellow). (d) 2d structure of the SVMP protein bound to hinokinin. (e) 3d structure of the SVMP protein (green) bound to ishwarol (blue). (f) 2d structure of the SVMP protein bound to ishwarol.

L-Amino Acid Oxidase

The 3D and 2D structures of LAAO bound to cubebin are shown in Figure 7(A) and (B), respectively. The major amino acids involved in the protein–ligand complex are Arg90, Glu219, Ser220, Phe227, Arg322, His463, and Gly464.

© STM Journals 2026. All Rights Reserved

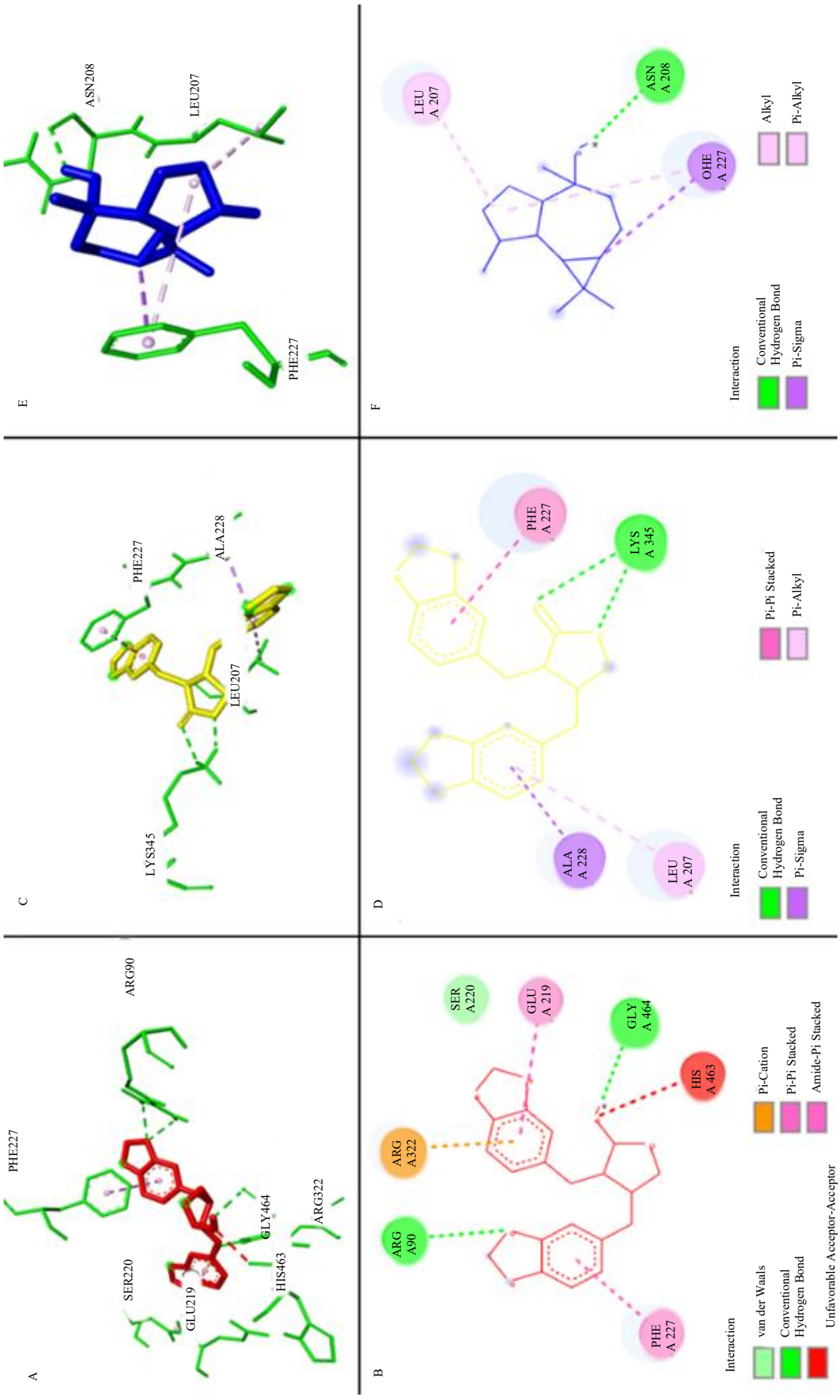

Figure 7. (a) 3d structure of the LAAO protein (green) bound to cubebin (red). (b) 2d structure of the LAAO protein bound to cubebin. (c) 3d structure of the LAAO protein (green) bound to hinokinin (yellow). (d) 2d structure of the LAAO protein bound to hinokinin. (e) 3d structure of the LAAO protein (green) bound to ledol (blue). (f) 2d structure of the LAAO protein bound to ledol.

© STM Journals 2026. All Rights Reserved

The 3D and 2D structures of LAAO bound to hinokinin are shown in Figure 7(C) and (D), respectively. The major amino acids involved in the protein–ligand complex are Leu207, Phe227, Ala228, and Lys345.

The 3D and 2D structures of LAAO bound to ledol are shown in Figure 7(E) and (F), respectively. The major amino acids involved in the protein–ligand complex are Leu207, Asn208, and Phe227.

Three-Finger Toxins

The 3D and 2D structures of 3FTx bound to hinokinin are shown in Figure 8(A) and (B), respectively. The major amino acids involved in the protein–ligand complex are Lys5, Cys41, Cys43, and Pro44.

The 3D and 2D structures of 3FTx bound to cubebin are shown in Figure 8(C) and (D), respectively. The major amino acids involved in the protein–ligand complex are Lys5, Pro18, Glu21, Tyr25, Cys41, Cys43, and Pro44.

The 3D and 2D structures of 3FTx bound to ishwarol are shown in Figure 8(E) and (F), respectively. The major amino acids involved in the protein–ligand complex are Asn26, Phe28, and Tyr53.

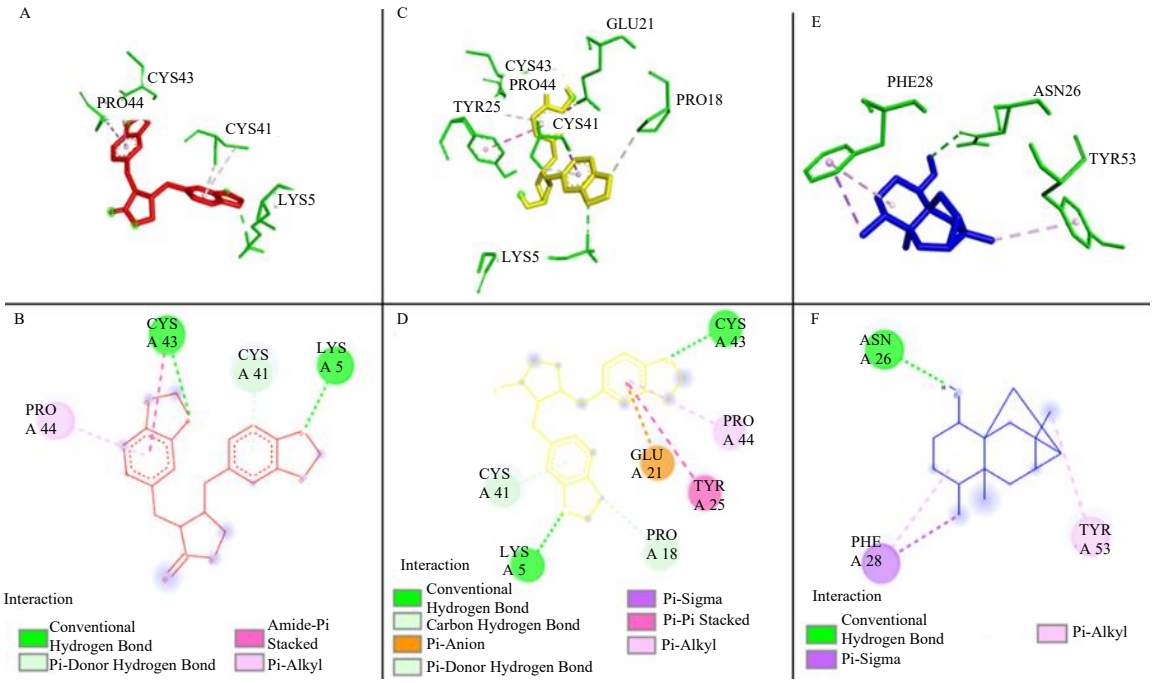

Figure 8. (a) 3d structure of the 3FTx protein (green) bound to hinokinin (red). (b) 2d structure of the 3FTx protein bound to hinokinin. (c) 3d structure of the 3FTx protein (green) bound to cubebin (yellow). (d) 2d structure of the 3FTx protein bound to cubebin. (e) 3d structure of the 3FTx protein (green) bound to ishwarol (blue). (f) 2d structure of the 3FTx protein bound to ishwarol.

Molecular Dynamics Simulations

From the results of molecular docking, the venom protein–ligand complex with the highest binding affinity, i.e., LAAO and cubebin, was taken for molecular dynamics simulations to evaluate the binding interactions in a biological system. Through trajectory analysis using MDS, the RMSD, RMSF, ROG, H-bonding, and solvent-accessible surface area (SASA) of the protein–ligand complex were determined.

RMSD

The protein complex denaturation and stability are determined using RMSD. Figure 9(A) illustrates the LAAO–cubebin complex over 100 ns. The complex showed an average RMSD of 0.16 nm, with

© STM Journals 2026. All Rights Reserved

the RMSD ranging from 0.1 to 0.15 nm for the initial 30 ns and only deviating to 0.16–0.175 nm from 30 to 100 ns. This shows the structural integrity of the complex.

RMSF

RMSF provides flexibility of residues while LAAO binds to cubebin. The complex had an average value of 0.1 nm, where it varied between 0.05 and 0.15 nm throughout the simulation, with the greatest fluctuation of 0.2 nm between residues 20 and 25 and another peak of 0.25 nm at residue 270 (Figure 9(B).

Radius of Gyration

ROG gives the degree of compactness of the protein–ligand complex. From Figure 9(C), it can be observed that the complex does not have any major variations in the graph, although a slight increase in the ROG can be observed after 30 ns. However, overall, the average ROG was observed as 2.87 nm.

Hydrogen Bonds

The number of hydrogen bonds gives an understanding of the interactions between the biomolecules. The average number of H-bonds was calculated as 720 from Figure 9(D), and no major fluctuations were observed in the graph.

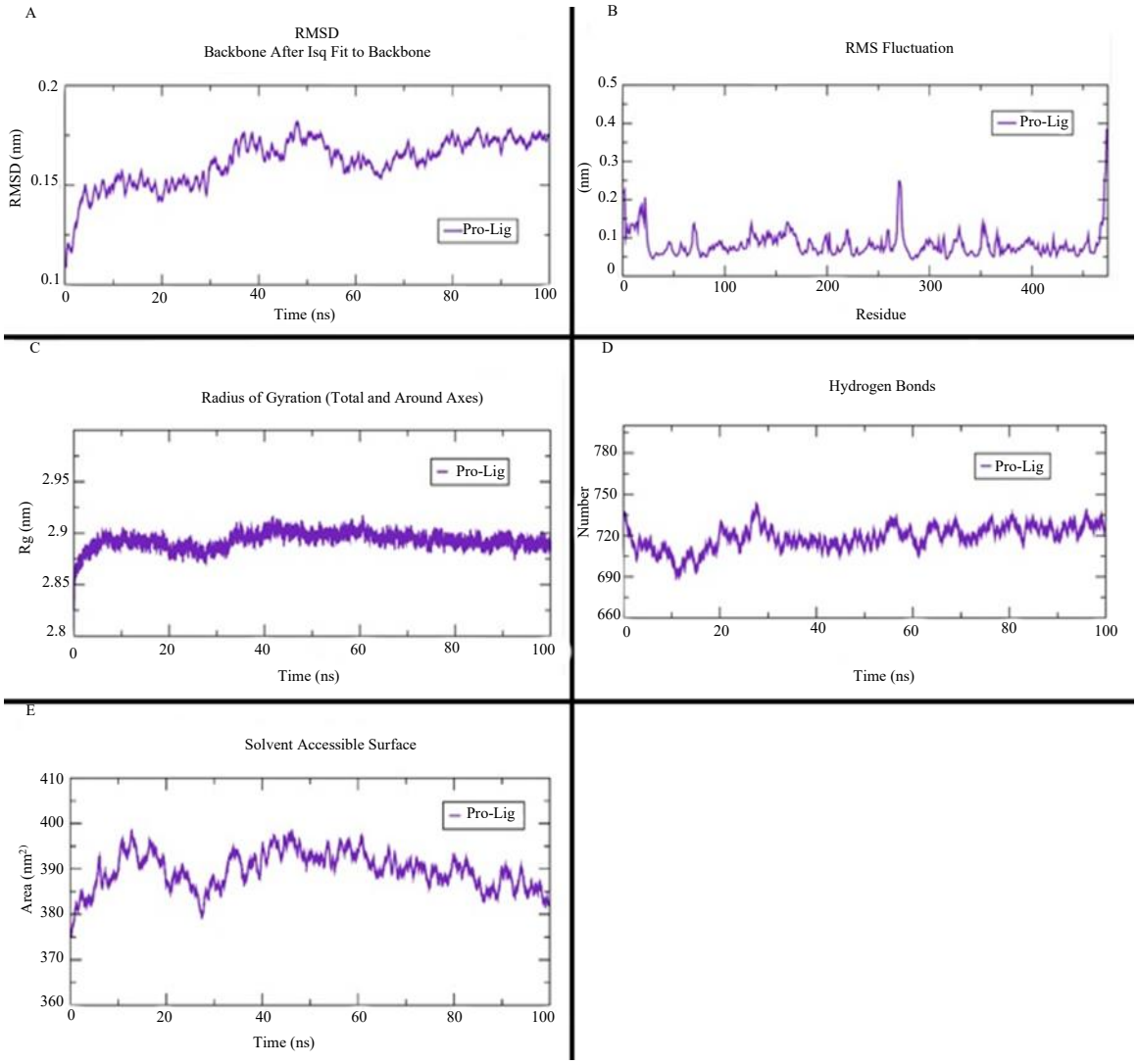

Figure 9. Results from molecular dynamics simulations of the LAAO–cubebin complex. (a) rmsd. (b) rmsf. (c) radius of gyration. (d) number of hydrogen bonds. (e) solvent-accessible surface area.

© STM Journals 2026. All Rights Reserved

Solvent-Accessible Surface Area

SASA is an important variable in analyzing protein folding and stability, which determines the interactions between the protein complex and the surrounding solvent. From Figure 9(E), the average SASA was found to be 390 nm², indicating that the interaction with the surrounding solvent is stable and exposes sufficient residues to interact with the solvent.

DISCUSSION

Snakebite envenomation is a significant threat to health, particularly to people living in the tropics, causing considerable cases of morbidity and mortality [16]. There are around 1.8–2.7 million instances of envenomation, ultimately leading to about 81,000–138,000 deaths each year [16]. SV is considered an adaptive evolutionary innovation of the salivary glands, consisting of a mixture of proteins and polypeptides capable of engaging in a variety of biological activities [17]. The heterogeneity and composition of these proteins make it difficult to treat these toxins. Therefore, in this study, phytocompounds in *A. indica* that could have possible venom-inhibiting properties were sought.

An ADME analysis using SwissADME was performed to identify compounds with drug-like properties. It was found that several of the 58 compounds were capable of exhibiting physicochemical drug-like properties and followed Lipinski's rule of five [15]. However, only five compounds had high BBB permeation, high GI absorption, and zero violations of the PAINS and BRENK alerts. In the case of venom proteins, as they affect the human biological system by interrupting neurotransmission through presynaptic and postsynaptic sites, BBB permeation is essential for the drug. Moreover, a drug, when ingested orally, must possess high GI tract absorption and solubility to exert optimal drug action. The five compounds (cubebin, hinokinin, ishwarol, and ledol) showed zero violations of the PAINS and BRENK alerts, indicating a prominent sign of accuracy and the less toxic nature of the compounds [18]. The toxicity of the compounds was further assessed using the ProTox-II tool and was placed under "class 4" of five classes (one being most toxic and five being least), which is considered moderate-to-low toxic. The screened compounds were also non-substrates for PGP, which indicates that the drug is not likely to be transported to the GI lumen, improving the bioavailability of the drug [19].

To progress to in silico studies, the structure of the amino acids of the purified proteins in the sterically permissible zone/favorable region must be greater than 90%. In this case, all four venom proteins have >90% of their amino acids in the permissible region. On performing docking, it was observed that the screened phytocompounds have strong hydrogen bonds to the active residues of the venom proteins. The structural biochemistry of PLA2 shows that the catalytic site exists in a tetrad of amino acids (His48, Asp49, Tyr52, and Asp99) and that the Ca2+-binding loop contains Tyr28, Gly30, Gly32, and Asp99 [20, 21]. The results show that the three compounds interact with His47, Asp48, and Gly29 (i.e., His48, Asp49, and Gly30, as a possible change in the reading frame). In the case of SVMPs, the zinc ion in the active site is coordinated by the amino acids His142, His146, and His152 [22]. Moreover, SVMP inhibitors have been previously known to affect the amino acids Ile108 and Leu170 by altering the catalytic site [23]. The least studied enzymes are LAAOs, yet they are an important constituent of snake venom. Studies have shown that LAAO inhibitors, like aristolochic acid and suramin, act by binding to Arg90, Leu207, Asn208, Phe227, His233, Arg322, and Lys345, whereas Gly464 is involved in substrate–ligand binding [24]. The screened phytocompounds interacted with the same residues, suggesting inhibition. The amino acids involved in the catalytic function of 3FTx enzymes could not be found, but studies have shown that the amino acids Tyr25, Cys41, and Pro44 are important in the formation of beta-sheets [25]. Although in the *Naja* genus, Lys5 is involved in forming a cationic cluster with other positively charged amino acids, which enhances the erythrocyte lytic activity in 3FTx proteins [26].

Following docking, the top candidate protein–ligand complex, i.e., LAAO–cubebin, was considered for molecular dynamics simulations. MD provides an effective method to analyze the dynamic nature of a protein and its interactions with a ligand. The stability of the drug–target protein is crucial in expediting the drug discovery process [27]. The trajectories of the simulated complex were used to

© STM Journals 2026. All Rights Reserved

investigate RMSD, RMSF, ROG, SASA, and H-bonds, providing valuable insight into the stability of the complex. RMSD provides insight into the stability and denaturation status of the complex, and 3.0 Å or 0.3 nm is considered an acceptable range for RMSD; i.e., lower the RMSD, the more stable the complex [27]. The results show an average RMSD of 0.16 nm without major deviations (Figure 9(A)) indicating that the complex is very stable. RMSF contributes to understanding the flexibility of each residue, providing insight into the stability of important sites of proteins such as the active site [28]. The average RMSF was found to be 0.1 nm, and fluctuations were observed between residue 20 and 25 and the 270th residue (Figure 9(B)). As mentioned in the previous paragraph, these residues are not important, and the fluctuations are not likely to affect stability. The compactness of protein–ligand complexes is assessed through ROG, and variations indicate less stability and compactness [27]. As seen in Figure 9(C), the graph showed little variation, with an average of 2.87 nm, further demonstrating the stability of the complex. The H-bonds and SASA are crucial in understanding the interactions between molecules in the complex and the surrounding solvent to maintain the stability of the complex [29]. An average of 720 H-bonds and a SASA of 390 nm^2 with no variations in the graph were observed, indicating good stability of the complex. Although it would have been ideal to compare these variables with the native protein.

From the molecular docking results, it is evident that the phytocompounds cubebin, hinokinin, ishwarol, and ledol show high binding affinities to all four venom proteins, especially hinokinin and cubebin. Moreover, MDS results revealed that the LAAO–cubebin complex was stable. In this study, only the molecular dynamics of the LAAO–cubebin complex could be studied due to funding restraints, but future studies can focus on the other venom protein–ligand complexes mentioned in this study. These compounds show promising results and have not been studied extensively with respect to their antivenom capabilities. Although the results show high binding affinity, the inhibitory ability of these compounds needs to be further evaluated.

CONCLUSION

Aristolochia indica is a medicinal plant used since ancient times by various South Indian tribes for the treatment of snakebites and scorpion bites. Much attention has been paid to aristolochic acid being efficacious against snake venom, but studies have proven the compound to be carcinogenic. From this study, it was revealed that *A. indica* contains unexplored phytocompounds with respect to its antivenom properties, namely, cubebin, hinokinin, ishwarol, and ledol. These compounds were screened from 58 phytocompounds from the plant that have drug-like properties through an ADME analysis and toxicology study. The compounds displayed ideal physicochemical properties, BBB permeation, and GI absorption; followed Lipinski's rule of five; and had zero violations of the PAINS and BRENK alerts. Furthermore, molecular docking was performed, which found that these five compounds have a high binding affinity to the major venom proteins (PLA2, SVMP, LAAO, and 3FTx), indicating their potential to act as an antivenom drug. Although the in silico analysis predicts the drug-likeness of these compounds, it only provides a static representation of binding. Molecular dynamics simulations demonstrated that the LAAO–cubebin complex is highly stable and could serve the purpose. Further studies need to demonstrate the dynamic behaviour of the other venom protein–ligand complexes to assess their stability and chances of being considered as an antivenom drug. Also, further in vitro and in vivo studies are necessary to evaluate the phytocompounds' inhibitory potential.

Abbreviations

3FTx	3 Finger Toxins
A. indica	*Aristolochia indica*
AA	Aristolochic Acid
ADME	Absorption, Distribution, Metabolism, Excretion
BBB	Blood Brain Barrier
GI	Gastro-Intestinal

© STM Journals 2026. All Rights Reserved

H-bond	Hydrogen Bond
IMPPAT	Indian Medicinal Plants, Phytochemistry and Therapeutics
LAAO	L-Amino Acid Oxidases
MDS	Molecular Dynamics Simulations
PDB	Protein Data Bank
PGP	P-Glycoprotein
PLA2	Phospholipase A2
RMSD	Root Mean Square Deviation
RMSF	Root Mean Square Fluctuation
ROG	Radius of Gyration
SASA	Solvent Accessible Surface Area
SV	Snake Venom
SVMP	Snake Venom Metalloproteinases
SVSP	Snake Venom Serine Proteases

REFERENCES

1. Waheed H, Moin SF, Choudhary MI. Snake venom: From deadly toxins to life-saving therapeutics. Curr Med Chem. 2017;24(17). Available from: http://www.eurekaselect.com/152913/article.
2. Osipov A, Utkin Y. What are the neurotoxins in hemotoxic snake venoms? Int J Mol Sci. 2023;24(3):2919.
3. Casewell NR, Jackson TNW, Laustsen AH, Sunaga K. Causes and consequences of snake venom variation. Trends Pharmacol Sci. 2020;41(8):570–81.
4. Doley R, Kini RM. Protein complexes in snake venom. Cell Mol Life Sci. 2009;66(17):2851–71. doi: 10.1007/s00018-009-0050-2. Available from: https://pmc.ncbi.nlm.nih.gov/articles/PMC11115964/.
5. Sanhajariya S, Duffull SB, Isbister GK. Pharmacokinetics of snake venom. Toxins. 2018;10(2):73.
6. Kalogeropoulos K, Treschow AF, auf dem Keller U, Escalante T, Rucavado A, Gutiérrez JM, et al. Protease activity profiling of snake venoms using high-throughput peptide screening. Toxins. 2019;11(3):170.
7. Kini RM, Doley R. Structure, function and evolution of three-finger toxins: Mini proteins with multiple targets. Toxicon. 2010;56(6):855–67.
8. Kasturiratne A, Wickremasinghe AR, de Silva N, Gunawardena NK, Pathmeswaran A, Premaratna R, et al. The global burden of snakebite: A literature analysis and modelling based on regional estimates of envenoming and deaths. PLoS Med. 2008;5(11):e218.
9. Modak BK, Gorai P, Pandey DK, Dey A, Malik T. An evidence based efficacy and safety assessment of the ethnobiologicals against poisonous and non-poisonous bites used by the tribals of three westernmost districts of West Bengal, India: Anti-phospholipase A2 and genotoxic effects. PLoS One. 2020;15(11):e0242944.
10. Dey A, Hazra AK, Mukherjee A, Nandy S, Pandey DK. Chemotaxonomy of the ethnic antidote Aristolochia indica for aristolochic acid content: Implications of anti-phospholipase activity and genotoxicity study. J Ethnopharmacol. 2021;266:113416.
11. Padhy GK. A review of Aristolochia indica: Ethnomedicinal uses, phytochemistry, pharmacological and toxicological effects. Curr Tradit Med. 2021;7(3):372–86.
12. Bhattacharjee P, Bhattacharyya D. Characterization of the aqueous extract of the root of Aristolochia indica: Evaluation of its traditional use as an antidote for snake bites. J Ethnopharmacol. 2013;145(1):220–6.
13. Jejurikar BL, Rohane SH. Drug designing in discovery studio. 2021. Available from: https://www.indianjournals.com/ijor.aspx?target=ijor:ajrc&volume=14&issue=2&article=008

© STM Journals 2026. All Rights Reserved

14. Kondapuram SK, Sarvagalla S, Coumar MS. Docking-based virtual screening using PyRx tool: Autophagy target Vps34 as a case study. In: Molecular docking for computer-aided drug design. Elsevier; 2021. p. 463–77. Available from: https://www.sciencedirect.com/science/article/pii/B9780128223123000199.
15. Shafiq KM, Harish R. Identification of phytocompounds from Argemone mexicana as inhibitors of Epstein-Barr nuclear antigen to combat infectious mononucleosis. Innovare J Med Sci. 2023;9–14.
16. Ravi DA, Hwang DH, Mohan Prakash RL, Kang C, Kim E. Indian medicinal plant-derived phytochemicals as potential antidotes for snakebite: A pharmacoinformatic study of atrolysin inhibitors. Int J Mol Sci. 2024;25(23):12675.
17. Choudhury M, McCleary RJR, Kini RM, Velmurugan D. Orphan three-finger toxins bind at tissue factor–factor VIIa interface to inhibit factor X activation: Identification of functional site by docking. TH Open. 2018;2:e303–14.
18. Ononamadu CJ, Ibrahim A. Molecular docking and prediction of ADME/drug-likeness properties of potentially active antidiabetic compounds isolated from aqueous-methanol extracts of Gymnema sylvestre and Combretum micranthum. BioTechnologia. 2021;102(1):85–99.
19. Wessler JD, Grip LT, Mendell J, Giugliano RP. The P-glycoprotein transport system and cardiovascular drugs. J Am Coll Cardiol. 2013;61(25):2495–502.
20. Trento MVC, Sales TA, De Abreu TS, Braga MA, Cesar PHS, Marques TR, et al. Exploring the structural and functional aspects of the phospholipase A2 from Naja spp. Int J Biol Macromol. 2019;140:49–58.
21. Yang CC. Structure-function relationship of phospholipase A2 from snake venoms. J Toxicol Toxin Rev. 1994;13(2):125–77.
22. Gomis-Rüth FX, Kress LF, Bode W. First structure of a snake venom metalloproteinase: A prototype for matrix metalloproteinases/collagenases. EMBO J. 1993;12(11):4151–7. doi: 10.1002/j.1460-2075.1993.tb06099.x. Available from: https://www.embopress.org/doi/epdf/10.1002/j.1460-2075.1993.tb06099.x.
23. Chellapandi P. Structural, functional and therapeutic aspects of snake venom metalloproteinases. Mini Rev Org Chem. 2014;11(1):28–44. doi: 10.2174/1570193X1101140402100707. Available from: https://www.benthamdirect.com/content/journals/mroc/10.2174/1570193X1101140402100707.
24. Ullah A. Structure–function studies and mechanism of action of snake venom L-amino acid oxidases. Front Pharmacol. 2020;11. Available from: https://www.frontiersin.org/journals/pharmacology/articles/10.3389/fphar.2020.00110/full.
25. Roy A, Zhou X, Chong MZ, D'hoedt D, Foo CS, Rajagopalan N, et al. Structural and functional characterization of a novel homodimeric three-finger neurotoxin from the venom of Ophiophagus hannah (king cobra). J Biol Chem. 2010;285(11):8302–15.
26. Kumar TKS, Jayaraman G, Lee CS, Arunkumar AI, Sivaraman T, Samuel D, et al. Snake venom cardiotoxins—Structure, dynamics, function and folding. J Biomol Struct Dyn. 1997;15(3):431–63.
27. Ogunyemi BT, Abdul-Hammed M, Adedotun IO, Egunjobi BT, Badmos ST, Adegboyega TA, et al. Protein–ligand molecular dynamics simulation (PL-MDS), ADMET analyses, and bioactivity studies of phytochemicals from Aloe vera: An in-silico novel antidiabetics drug discovery effort. Discov Chem. 2025;2(1):55.
28. Dasmahapatra U, Kumar CK, Das S, Subramanian PT, Murali P, Isaac AE, et al. In-silico molecular modelling, MM/GBSA binding free energy and molecular dynamics simulation study of novel pyrido fused imidazo[4,5-c]quinolines as potential anti-tumor agents. Front Chem. 2022;10:991369.
29. Dasmahapatra U, Kumar CK, Das S, Subramanian PT, Murali P, Isaac AE, et al. In-silico molecular modelling, MM/GBSA binding free energy and molecular dynamics simulation study of novel pyrido fused imidazo[4,5-c]quinolines as potential anti-tumor agents. Front Chem. 2022;10:991369.

© STM Journals 2026. All Rights Reserved